

# Origin of Drastic Change of Fermi Surface and Transport Anomalies in CeRhIn<sub>5</sub> under Pressure

Shinji WATANABE and Kazumasa MIYAKE

*Division of Materials Physics, Department of Materials Engineering Science, Graduate School of Engineering Science, Osaka University, Toyonaka, Osaka 560-8531, Japan*

The mechanism of drastic change of Fermi surfaces as well as transport anomalies near  $P = P_c \approx 2.35$  GPa in CeRhIn<sub>5</sub> is explained theoretically. The key mechanism is pointed out to be the interplay of magnetic order and Ce-valence fluctuations. We show that the antiferromagnetic state with “small” Fermi surfaces changes to the paramagnetic state with “large” Fermi surfaces with huge enhancement of effective mass of electrons with keeping finite c-f hybridization. This explains the drastic change of the de Haas-van Alphen signals. Furthermore, it is also consistent with the emergence of  $T$ -linear resistivity simultaneous with the residual resistivity peak at  $P = P_c$  in CeRhIn<sub>5</sub>.

KEYWORDS: CeRhIn<sub>5</sub>, Fermi surface, non-Fermi liquid, localized-itinerant transition, valence fluctuation

The mechanism of instability of electronic states emerging when the magnetically-ordered temperature is suppressed to absolute zero by tuning material parameters has been one of the central issues in condensed matter physics.<sup>1–3</sup> A heavy-electron metal CeRhIn<sub>5</sub> has been extensively studied as the prototypical material. Accumulated experiments, however, have revealed that the physics of CeRhIn<sub>5</sub> seem to be beyond conventional understanding<sup>1–3</sup> and require an essentially new concept.

CeRhIn<sub>5</sub> undergoes an antiferromagnetic (AF) transition at  $T_N = 3.8$  K with an ordered vector  $\mathbf{Q} = (1/2, 1/2, 0.297)$  at ambient pressure.<sup>4</sup> When pressure is applied under a magnetic field larger than the upper critical field, the AF order is suppressed at  $P = P_c \approx 2.35$  GPa.<sup>5–11</sup> Interestingly, a drastic change of Fermi surfaces was discovered at  $P = P_c$  by the de Haas-van Alphen (dHvA) measurement.<sup>9</sup> For  $0 \leq P < P_c$ , the main dHvA frequencies are in good agreement with those of LaRhIn<sub>5</sub> where the 4f electron is absent. On the other hand, for  $P > P_c$ , the dHvA frequencies were identified to be approximately the same as those of CeCoIn<sub>5</sub>, where 4f electrons are itinerant, contributing to the formation of the Fermi surface. The electrons on a typical Fermi surface, the cylindrical  $\beta_2$  branch, shows the mass enhancement from  $m^* = 6m_0$  at  $P = 0$  to  $60m_0$  at  $P \approx 2.2$  GPa with  $m_0$  being a free-electron mass.<sup>9</sup> For  $P > P_c$ , the dHvA signal of the  $\beta_2$  branch is lost probably because of a too-large effective mass close to  $100m_0$ , where the heavy-electron state is realized in the paramagnetic-metal phase.<sup>9</sup>

So far, it has been thought that this drastic change of the Fermi surfaces might be explained in terms of the “localized” to “itinerant” transition of f electrons.<sup>12</sup> However, this conception encounters a serious difficulty in elucidating the experimental fact that the effective mass of electrons is enhanced even at  $P = 0$  with the Sommerfeld constant  $\gamma \approx 56$  mJmol<sup>−1</sup>K<sup>−2</sup>,<sup>5</sup> which is about 10 times larger than that of LaRhIn<sub>5</sub>.<sup>13,14</sup>

Furthermore, resistivity measurements revealed that a striking anomaly emerges near  $P = P_c$ .<sup>7</sup> The low- $T$  re-

sistivity  $\rho(T = 2.25$  K) has a sharp peak at  $P = P_c$ , suggesting that the residual resistivity  $\rho_0$  is strongly enhanced near  $P = P_c$ .<sup>7,11,12</sup> The low-temperature resistivity also exhibits anomalous behavior: The  $T$ -linear resistivity  $\rho(T) \propto T$  emerges most prominently near  $P = P_c$  with a wide- $T$  range up to  $\sim 10$  K.<sup>7,11,12</sup> This behavior is quite different from that of normal metals described by the Fermi liquid  $\rho \propto T^2$  as well as the conventional quantum criticality scenario near the AF quantum critical point (QCP) in three dimension (3D)  $\rho \propto T^{1.5}$ .<sup>1–3</sup> The origin and mechanism of these transport anomalies as well as the drastic change of the Fermi surface at  $P = P_c$  accompanied by huge mass enhancement have not been clarified so far.

Recently, an important measurement has been performed under pressure and magnetic field.<sup>11</sup> G. Knebel *et al.* have measured the  $T^2$  coefficient  $A$  in the resistivity in the  $T \rightarrow 0$  limit at the magnetic field  $H = 15$  T, and found that  $A$  increases as pressure increases toward  $P = P_c$ . They have shown that under pressure,  $\sqrt{A}$  shows an enhancement similar to the effective mass of electrons  $m^*$  of the  $\beta_2$  branch obtained by the dHvA measurement,<sup>9</sup> satisfying the  $\sqrt{A}/m^* = \text{const.}$  scaling. This indicates that the mass enhancement is *not* caused by the quantum criticality of the AF spin fluctuations, since in the case of the 3D (2D) AF QCP,  $\sqrt{A}/m^*$  is expected to show the  $T^{-1/4}$  ( $T^{-1/2}$ ) divergence.<sup>1–3</sup> Namely, the  $\sqrt{A}/m^* = \text{const.}$  scaling strongly suggests that the mass enhancement near  $P = P_c$  purely comes from the band effect.

On the basis of these observations, in this Letter, we present a theoretical explanation for resolving this outstanding puzzle in CeRhIn<sub>5</sub>. We show that the drastic change of the Fermi surface from a “small” to a “large” one occurs at the phase transition from AF to paramagnetic metal with huge mass enhancement under pressure, as observed. An important point here is that these results are obtained with finite hybridization between f and conduction electrons, which overcomes the difficulty of conventional scenario that f electrons undergo “localized”

to “itinerant” transition.<sup>12</sup> Our result not only naturally explains the  $\sqrt{A}/m^* = \text{const.}$  scaling, but also gives the reason why the  $T$ -linear resistivity emerges as well as the residual resistivity has a peak in the vicinity of  $P = P_c$ .

Let us start our discussion by introducing a minimal model, which describes the essential part of the physics of CeRhIn<sub>5</sub>, in the standard notation:

$$H = H_c + H_f + H_{\text{hyb}} + H_{U_{fc}}, \quad (1)$$

where  $H_c = \sum_{\mathbf{k}\sigma} \varepsilon_{\mathbf{k}} c_{\mathbf{k}\sigma}^\dagger c_{\mathbf{k}\sigma}$  represents the conduction band,  $H_f = \varepsilon_f \sum_{i\sigma} n_{i\sigma}^f + U \sum_{i=1}^N n_{i\uparrow}^f n_{i\downarrow}^f$  the  $f$  level and onsite Coulomb repulsion for  $f$  electrons,  $H_{\text{hyb}} = V \sum_{i\sigma} (f_{i\sigma}^\dagger c_{i\sigma} + c_{i\sigma}^\dagger f_{i\sigma})$  the hybridization between  $f$  and conduction electrons, and  $H_{U_{fc}} = U_{fc} \sum_{i=1}^N n_i^f n_i^c$  the Coulomb repulsion between  $f$  and conduction electrons, respectively. The  $H_{U_{fc}}$  term is a key parameter for explaining the anomalous transport properties of CeRhIn<sub>5</sub>; The  $\rho_0$  peak and  $\rho \propto T$  observed in CeRhIn<sub>5</sub> are quite similar to the observations in CeCu<sub>2</sub>Ge<sub>2</sub>,<sup>15</sup> CeCu<sub>2</sub>Si<sub>2</sub>,<sup>16</sup> and CeCu<sub>2</sub>(Si<sub>x</sub>Ge<sub>1-x</sub>)<sub>2</sub>.<sup>17</sup> The pressure dependence of the coefficient  $A$ <sup>15–17</sup> as well as the Cu-NQR frequency<sup>18</sup> strongly suggest that these anomalies occur at the pressure where the valence of Ce changes sharply. The Ce-valence transition is well known as the  $\gamma$ - $\alpha$  transition in Ce metal. Band-structure calculation for Ce metal showed that 4 $f$ - and 5 $d$ -electron bands are located at the Fermi level.<sup>19</sup> Since both the orbitals are located at the same Ce site, the inter-orbital Coulomb repulsion  $U_{fc}$  has a considerable magnitude, causing the first-order valence transition.<sup>20,21</sup> Although  $U_{fc}$  is considered to be rather moderate in Ce compounds, valence fluctuations still affect physical quantities significantly even in such a valence-crossover regime.<sup>21–24</sup> Theoretical calculations based on the model (1) have shown that strong Ce-valence fluctuations cause the enhancement of the residual resistivity<sup>25</sup> as well as the  $T$ -linear resistivity.<sup>16</sup>

Since the  $\rho_0$  peak and  $\rho \propto T$  appear just at the boundary between the AF and paramagnetic phases,  $P \approx P_c$ , in CeRhIn<sub>5</sub>, the interplay of AF and the Ce-valence fluctuation seems to be a key mechanism.<sup>8</sup> To treat both effects on equal footing, we apply the slave-boson mean-field theory<sup>26</sup> to Eq. (1). We use the hybridization form  $V Z_{i\sigma} f_{i\sigma}^\dagger c_{i\sigma}$  instead of  $V f_{i\sigma}^\dagger c_{i\sigma}$  in Eq. (1) by introducing bose creation (annihilation) operators  $e_i^\dagger(e_i)$  and  $d_i^\dagger(d_i)$  for the empty and doubly-occupied states, respectively, and  $p_{i\uparrow}^\dagger(p_{i\uparrow})$  and  $p_{i\downarrow}^\dagger(p_{i\downarrow})$  for singly-occupied states by requiring the constraint for completeness condition  $\sum_i \lambda'_i (e_i^\dagger e_i + p_{i\uparrow}^\dagger p_{i\uparrow} + p_{i\downarrow}^\dagger p_{i\downarrow} + d_i^\dagger d_i - 1)$  and  $\sum_{i\sigma} \lambda_{i\sigma} (f_{i\sigma}^\dagger f_{i\sigma} - p_{i\sigma}^\dagger p_{i\sigma} - d_i^\dagger d_i)$  with  $\lambda'_i$  and  $\lambda_{i\sigma}$  being the Lagrange multipliers. Here, the renormalization factor for hybridization is defined as  $Z_{i\sigma} \equiv (1 - d_i^\dagger d_i - p_{i\sigma}^\dagger p_{i\sigma})^{-1/2} (e_i^\dagger e_i + p_{i-\sigma}^\dagger p_{i-\sigma})^{-1/2}$ . To capture the essence of CeRhIn<sub>5</sub> as noted later, we consider the commensurate AF order on a bipartite lattice and consider  $\lambda_{ia\sigma}$  and  $\lambda_{ib\sigma}$  corresponding to the two sublattice ( $ia$  and  $ib$  sites) instead of  $\lambda_{i\sigma}$ , which are expressed as  $\lambda_{ia\uparrow} = \lambda_{ib\downarrow} \equiv \lambda_i + \delta\lambda_i$ ,  $\lambda_{ia\downarrow} = \lambda_{ib\uparrow} \equiv \lambda_i - \delta\lambda_i$ , respectively. For  $H_{U_{fc}}$  in Eq. (1), we employ the mean-field decoupling as  $n_i^f n_i^c \simeq \bar{n}_f n_i^c + \bar{n}_c n_i^f - \bar{n}_f \bar{n}_c$  with

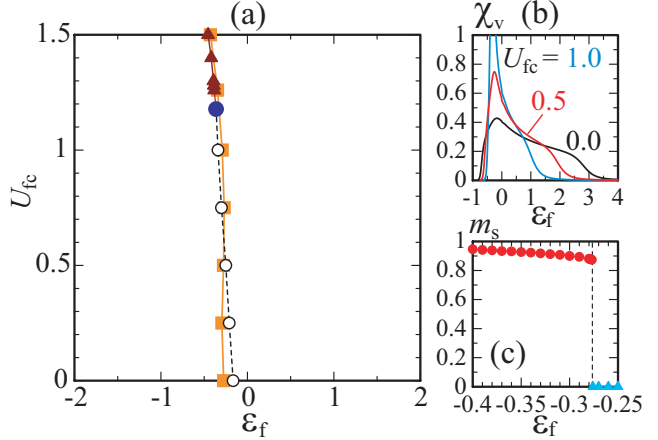


Fig. 1. (color online) (a) Ground-state phase diagram in the plane of  $U_{fc}$  and  $\varepsilon_f$  for paramagnetic and AF states (see text). The first-order valence-transition line (solid line with triangles) terminates at the quantum critical point (filled circle). The valence crossover occurs at the dashed line with open circles, at which  $\chi_v$  has a maximum, as shown in (b). The solid line with filled squares represents the boundary between the AF state and the paramagnetic state (see text). (c) The AF order parameter  $m_s$  vs.  $\varepsilon_f$  for  $U_{fc} = 0.5$ . All results in (a)-(c) are calculated for  $t = 1$ ,  $V = 0.2$ , and  $U = \infty$  at  $n = 0.9$ .

$\bar{n}_f \equiv \sum_i \langle n_i^f \rangle / N$  and  $\bar{n}_c \equiv \sum_i \langle n_i^c \rangle / N$ . By approximating mean fields and Lagrange multipliers as uniform ones, i.e.,  $e = \langle e_i \rangle$ ,  $p_\sigma = \langle p_{i\sigma} \rangle$ , and  $d = \langle d_i \rangle$ ,  $\lambda' = \lambda'_i$ ,  $\delta\lambda = \delta\lambda_i$ , and  $\lambda = \lambda_i$ , respectively, the set of mean-field equations is obtained by optimal conditions  $\partial \langle H \rangle / \partial x = 0$  for  $x = \lambda', \delta\lambda, \lambda, e, d, p_\uparrow$ , and  $p_\downarrow$ :

$$\begin{aligned} e^2 + p_\uparrow^2 + p_\downarrow^2 + d^2 - 1 &= 0, \\ p_\uparrow^2 - p_\downarrow^2 &= \frac{2}{N} \sum_{\mathbf{k}} \left[ \langle f_{\mathbf{k}\uparrow}^\dagger f_{\mathbf{k}+\mathbf{Q}\uparrow} \rangle - \langle f_{\mathbf{k}\downarrow}^\dagger f_{\mathbf{k}+\mathbf{Q}\downarrow} \rangle \right], \\ p_\uparrow^2 + p_\downarrow^2 + 2d^2 &= \frac{1}{N} \sum_{\mathbf{k}\sigma} \left[ \langle f_{\mathbf{k}\sigma}^\dagger f_{\mathbf{k}\sigma} \rangle + \langle f_{\mathbf{k}+\mathbf{Q}\sigma}^\dagger f_{\mathbf{k}+\mathbf{Q}\sigma} \rangle \right], \\ \frac{V}{N} \sum_{\mathbf{k}\sigma} \left( \frac{\partial Z_\sigma}{\partial e} \right) \left[ \langle f_{\mathbf{k}\sigma}^\dagger c_{\mathbf{k}\sigma} \rangle + \langle f_{\mathbf{k}+\mathbf{Q}\sigma}^\dagger c_{\mathbf{k}+\mathbf{Q}\sigma} \rangle \right] + \lambda' e &= 0, \\ \frac{V}{N} \sum_{\mathbf{k}\sigma} \left( \frac{\partial Z_\sigma}{\partial d} \right) \left[ \langle f_{\mathbf{k}\sigma}^\dagger c_{\mathbf{k}\sigma} \rangle + \langle f_{\mathbf{k}+\mathbf{Q}\sigma}^\dagger c_{\mathbf{k}+\mathbf{Q}\sigma} \rangle \right] + (U + \lambda' - 2\lambda) d &= 0, \\ \frac{V}{N} \sum_{\mathbf{k}\sigma} \left( \frac{\partial Z_\sigma}{\partial p_\uparrow} \right) \left[ \langle f_{\mathbf{k}\sigma}^\dagger c_{\mathbf{k}\sigma} \rangle + \langle f_{\mathbf{k}+\mathbf{Q}\sigma}^\dagger c_{\mathbf{k}+\mathbf{Q}\sigma} \rangle \right] + (\lambda' - \lambda - \delta\lambda) p_\uparrow &= 0, \\ \frac{V}{N} \sum_{\mathbf{k}\sigma} \left( \frac{\partial Z_\sigma}{\partial p_\downarrow} \right) \left[ \langle f_{\mathbf{k}\sigma}^\dagger c_{\mathbf{k}\sigma} \rangle + \langle f_{\mathbf{k}+\mathbf{Q}\sigma}^\dagger c_{\mathbf{k}+\mathbf{Q}\sigma} \rangle \right] + (\lambda' - \lambda + \delta\lambda) p_\downarrow &= 0, \end{aligned}$$

where  $\mathbf{Q}$  is the AF-ordered vector. Here,  $\sum_{\mathbf{k}}$  denotes the summation over the 1st Brillouin zone. The chemical potential  $\mu$  is determined so as to give the total filling  $n = (\bar{n}_f + \bar{n}_c)/2$  with  $\bar{n}_f + \bar{n}_c = \frac{1}{N} \sum_{\mathbf{k}\sigma} [\langle f_{\mathbf{k}\sigma}^\dagger f_{\mathbf{k}\sigma} \rangle + \langle f_{\mathbf{k}+\mathbf{Q}\sigma}^\dagger f_{\mathbf{k}+\mathbf{Q}\sigma} \rangle + \langle c_{\mathbf{k}\sigma}^\dagger c_{\mathbf{k}\sigma} \rangle + \langle c_{\mathbf{k}+\mathbf{Q}\sigma}^\dagger c_{\mathbf{k}+\mathbf{Q}\sigma} \rangle]$ . These equations are solved self-consistently.

To clarify the mechanism of drastic change of the Fermi surface of CeRhIn<sub>5</sub>, the most typical one, the two-dimensional-like Fermi surface, observed as the  $\beta_2$  branch, we consider  $\varepsilon_{\mathbf{k}} = -2t(\cos k_x + \cos k_y)$  on the square lattice. Hereafter, the energy unit is taken as  $t = 1$ . To simulate the AF order in the heavy-electron state realized in CeRhIn<sub>5</sub>, we consider the small hybridization  $V = 0.2$  case near half filling  $n = 0.9$ , and the AF order with  $\mathbf{Q} = (\pi, \pi)$ . Although we here cal-

culated several  $U$  cases, we show the result for  $U = \infty$ , since the result is essentially unchanged even for finite  $U$ , as far as  $U$  is larger than the bandwidth.

First, we show the ground-state phase diagram determined under the assumption of the paramagnetic states with  $p_\uparrow = p_\downarrow$  and  $\delta\lambda = 0$  in Fig. 1(a). The first-order valence transition line (solid line with filled triangles) terminates at the QCP (filled circle) at  $(\varepsilon_f^{\text{QCP}}, U_{\text{fc}}^{\text{QCP}}) = (-0.3623, 1.1778)$ . For  $U_{\text{fc}} > U_{\text{fc}}^{\text{QCP}}$ ,  $\bar{n}_f$  shows a jump as a function of  $\varepsilon_f$ , indicating the first-order transition between the paramagnetic metals with  $\bar{n}_f$  close to 1 and  $\bar{n}_f < 1$  in deep- $\varepsilon_f$  and shallow- $\varepsilon_f$  regions, respectively, since large  $U_{\text{fc}}$  forces electrons to pour into either the f level or the conduction band.<sup>20–22,24</sup> At the QCP, valence fluctuations diverge  $\chi_v = -\partial\bar{n}_f/\partial\varepsilon_f = \infty$ , and for  $U_{\text{fc}} < U_{\text{fc}}^{\text{QCP}}$ ,  $\chi_v$  has a conspicuous peak at  $\varepsilon_f$  represented by the dashed line with open circles in Fig. 1(a), indicating strong valence fluctuations, as shown in Fig. 1(b). At the QCP, the characteristic energy scale of the system, the so-called Kondo temperature is given by  $T_K \equiv \bar{\varepsilon}_f - \mu = 2.93 \times 10^{-3}$  with  $\bar{\varepsilon}_f = \varepsilon_f + \lambda + U_{\text{fc}}\bar{n}_c$ .

When the AF states are taken into account, the AF order parameter defined as  $m_s \equiv p_\uparrow^2 - p_\downarrow^2$  decreases as  $\varepsilon_f$  increases, as shown in Fig. 1(c) for  $U_{\text{fc}} = 0.5$ . When the ground-state energies of this AF state and the paramagnetic state are compared, the level crossing occurs at  $\varepsilon_f = \varepsilon_f^c$ . Then, this AF and paramagnetic phase transition is identified to be of the first order. The phase boundary determined in this way is shown by the solid line with filled squares in Fig. 1(a). We find that the AF order terminates in the vicinity of the first-order valence transition line and the valence-crossover line. These results imply that the suppression of the AF order occurs at the points with strong valence fluctuations.

These results are favorably compared with CeRhIn<sub>5</sub>. Applying pressure to Ce systems corresponds to increasing  $\varepsilon_f$ , since negative ions approach the tail of 4f wavefunction at the Ce site. Experimental fact of the sudden disappearance of the AF order at  $P = P_c$  and simultaneous emergence of the  $\rho_0$  peak as well as  $\rho \propto T$  near  $P = P_c$  seem to be well described by the results shown in Fig. 1: The vicinity of  $\varepsilon_f^c$  for moderate  $U_{\text{fc}} (< U_{\text{fc}}^{\text{QCP}})$  with well-developed  $\chi_v$  seems to correspond to the vicinity of  $P = P_c$  in CeRhIn<sub>5</sub>.

To analyze the Fermi-surface change shown by the dHvA measurement in CeRhIn<sub>5</sub>, we apply the magnetic field to Eq. (1) as  $-\hbar \sum_i (S_i^{fz} + S_i^{cz})$ . The dHvA effect<sup>9</sup> and  $A$  coefficient<sup>11</sup> were measured at  $H = 12 \sim 17$  T and  $H = 15$  T, respectively. The magnetic field of  $H = 15$  T is estimated to be  $h = 0.0046t$  when the half bandwidth of the conduction band  $4t$  of Eq. (1) is compared with that of CeRhIn<sub>5</sub> by the band-structure calculation, about 1.5 eV.<sup>27</sup> Then, we show in Fig. 2 the contour plot of the energy band of Eq. (1) with  $\downarrow$  spin located at the Fermi level  $\mu$  for  $U_{\text{fc}} = 0.5$  at  $h = 0.005$ .

In the AF state, the lower hybridized band of Eq. (1) is folded, giving rise to the hole region emerging at the magnetic zone boundary connecting  $\mathbf{k} = (0, \pi)$  and  $(\pi, 0)$ , as shown in Fig. 2(a). Here, in order to make a comparison with the “small” Fermi surface, which consists of

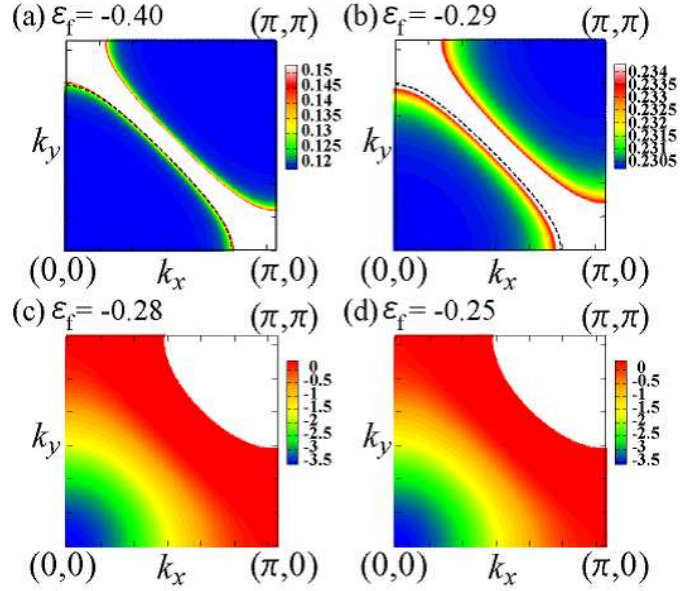


Fig. 2. (color online) The contour plot of the energy band with  $\downarrow$  spin located at the Fermi level  $\mu$  for  $t = 1$ ,  $V = 0.2$ ,  $U = \infty$ ,  $U_{\text{fc}} = 0.5$ , and  $n = 0.9$  at  $h = 0.005$ : (a)  $\varepsilon_f = -0.40$ , (b)  $\varepsilon_f = -0.29$ , (c)  $\varepsilon_f = -0.28$ , and (d)  $\varepsilon_f = -0.25$ . The  $E_{\mathbf{k}\downarrow} > \mu$  parts are represented by white regions. In (a) and (b), the dashed line indicates the Fermi surface of the conduction band,  $\varepsilon_{\mathbf{k}}$  for  $\bar{n}_c = 0.8$ .

only conduction electrons, we plot the Fermi surface of the conduction band  $\varepsilon_{\mathbf{k}}$  at the filling  $\bar{n}_c = 0.8$  as the dashed line in Fig. 2(a). This Fermi surface corresponds to that when the hybridization between f and conduction electrons is switched off,  $V = 0$  in Eq. (1); Since f electrons for  $\bar{n}_f = 1$  are located at the localized f level for  $V = 0$ , extra electrons in  $n = 0.9$ , i.e.,  $\bar{n}_c = 0.8$  are in the conduction band. We see that the Fermi surface of the AF state for  $V = 0.2$  is nearly the same as the “small” Fermi surface represented by the dashed line. This corresponds to the experimental fact that the dHvA signals of CeRhIn<sub>5</sub> are very similar to those of LaRhIn<sub>5</sub> in the AF-ordered phase for  $P \leq P_c$ .<sup>9,13</sup>

The shape of the Fermi surface close to the “small” Fermi surface remains until  $\varepsilon_f$  reaches the AF-paramagnetic boundary  $\varepsilon_f^c = -0.283$ , as shown in Fig. 2(b), which corresponds to CeRhIn<sub>5</sub> at  $P \lesssim P_c$ . When  $\varepsilon_f$  exceeds  $\varepsilon_f^c$ , the Fermi surface drastically changes, as shown in Fig. 2(c) for  $\varepsilon_f = -0.280$ ; The folding of the lower hybridized band disappears and the “large” Fermi surface recovers, which is clearly different from the “small” Fermi surface shown in Figs. 2(a) and (b). This “large” Fermi surface remains in the paramagnetic phase, as shown in Fig. 2(d) for  $\varepsilon_f = -0.250$ .

To facilitate the comparison with the dHvA result, we plot the Fermi wave number  $k_F$ , defined by the distance between  $\mathbf{k} = (0, 0)$  and the intersection point of the Fermi surface and the line connecting  $\mathbf{k} = (0, 0)$  and  $(\pi, \pi)$ , in Fig. 3(a). Here, for the AF-ordered state  $\varepsilon_f < \varepsilon_f^c$ ,  $k_F$  in the 1st Brillouin zone is plotted. We see that  $k_F$  is almost unchanged as a function of  $\varepsilon_f$ , which is nearly the same as  $k_F$  of the conduction band at  $\bar{n}_c = 0.8$ ,  $k_F^c$  represented by the solid line. Then,  $k_F$  shows an abrupt jump at  $\varepsilon_f^c$ . This

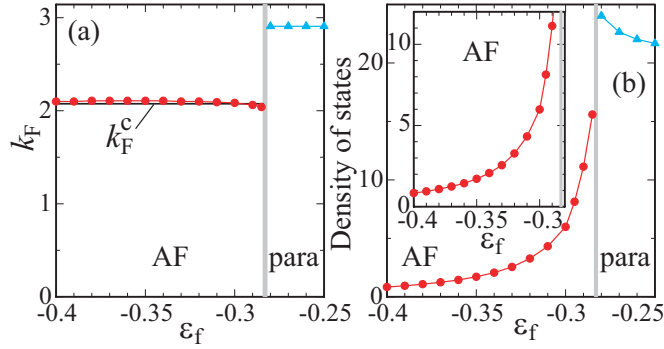


Fig. 3. (color online) (a) Fermi wavenumber  $k_F$  vs.  $\epsilon_f$  in the AF state (circles) and the paramagnetic state (triangles) for  $t = 1$ ,  $V = 0.2$ ,  $U = \infty$ ,  $U_{fc} = 0.5$ , and  $h = 0.005$  at  $n = 0.9$ . The solid line represents  $k_F$  for the conduction band  $\epsilon_k$  at  $n_c = 0.8$ . (b)  $D(\mu)$  vs.  $\epsilon_f$  for the same parameters as (a). Inset is enlargement of the AF phase.

is quite consistent with the dHvA measurement that the dHvA frequencies, including the  $\beta_2$  branch, keep almost constant for  $0 \leq P < P_c$ , and they suddenly jump at  $P = P_c$  and remain constant for  $P > P_c$ .

We find that the measured enhancement of the effective mass of electrons from  $m^* \sim 6m_0$  at  $P = 0$  to  $m^* \sim 60m_0$  at  $P \rightarrow P_c$ <sup>9</sup> is also reproduced; The  $\epsilon_f$  dependence of the density of states (DOS) at the chemical potential  $\mu$ ,  $D(\mu)$ , is shown in Fig. 3(b), where  $D(\omega) \equiv \sum_{\mathbf{k}\sigma} \delta(\omega - E_{\mathbf{k}\sigma}) / (2N)$  with  $E_{\mathbf{k}\sigma}$  being the energy band of Eq. (1). The DOS is enhanced about 10 times when  $\epsilon_f$  approaches  $\epsilon_f^c$ , as shown in the inset of Fig. 3(b). However, the renormalization factor  $\sqrt{Z_\sigma}$ , due to the many-body effect, does not show divergent growth even as  $\epsilon_f$  approaches  $\epsilon_f^c$ . This implies that the divergent growth of the DOS is mainly due to the band effect. Then,  $D(\mu)$  is proportional to  $m^*$  and  $\sqrt{A}$ , explaining the measured  $\sqrt{A}/m^* = \text{const.}$  scaling.<sup>11,28</sup> We note that  $D(\mu)$  at  $\epsilon_f = -0.4$  is about 10 times larger than the density of states of conduction electrons at  $n_c = 0.8$ ,  $D_c(\mu) = 0.092$ , which is also consistent with enhanced  $\gamma$  of CeRhIn<sub>5</sub><sup>5</sup> from that of LaRhIn<sub>5</sub><sup>13,14</sup> at  $P = 0$ . When  $\epsilon_f$  increases,  $m_s$  decreases, as shown in Fig. 1(c). Since the increase in  $\epsilon_f$  tends to increase the renormalization factor  $\sqrt{Z_\sigma}$ , the energy gap between the original lower-hybridized band and the folded band in the AF phase is increased. This effect pushes up the latter band in the 1st Brillouin zone, making the flat part of the band, mainly contributed from f electrons, whose bottom is located at  $\mathbf{k} = (0, 0)$  start to emerge at the Fermi level (see Fig. 2(b)).

In the paramagnetic phase for  $\epsilon_f > \epsilon_f^c$ ,  $D(\mu)$ 's have larger values than those in the AF phase, as shown in Fig. 3(b). The increase in the DOS toward  $\epsilon_f^c$  in the paramagnetic phase is naturally understood since as  $\epsilon_f$  decreases,  $\bar{n}_f$  increases to approach 1, i.e., the Kondo state, giving rise to the reduction of  $T_K$ , i.e., enhancement of  $D(\mu)$ . In CeRhIn<sub>5</sub>, the dHvA signal of the  $\beta_2$  branch has not been detected for  $P > P_c$ , probably because its effective mass is too large, close to  $100m_0$ .<sup>9</sup> This is also consistent with our result. For  $\epsilon_f > \epsilon_f^c$ ,  $D(\mu)$  decreases as  $h$  in-

creases. This is also consistent with the field-dependence of  $m^*$  of the  $\beta_2$  branch in CeCoIn<sub>5</sub>,<sup>29</sup> which is expected to correspond to the paramagnetic state of CeRhIn<sub>5</sub> for  $P > P_c$ .<sup>23,30</sup>

The increase in  $D(\mu)$  toward  $\epsilon_f^c$ , shown in Fig. 3(b), suggests that total DOS at the 3D Fermi surface of CeRhIn<sub>5</sub> gives rise to the measured peak structure of the  $A$  coefficient at  $P = P_c$ .<sup>11</sup> Our results clearly show that the “small” Fermi surface can be observed by dHvA measurement even without switching off the c-f hybridization, which reminds us of the elucidation of metamagnetism in CeRu<sub>2</sub>Si<sub>2</sub>.<sup>31–33</sup>

Recently, a possibility that the AF and paramagnetic transition is continuous under pressure has been reported by the In-NQR measurement at  $H = 0$ .<sup>34</sup> To clarify the detailed nature of the phase competition at the magnetic field smaller than the upper critical field,  $\sim 10$  T, existence of the superconductivity should be taken into account, which is out of scope of the present study.

In summary, we have shown that the drastic change of Fermi surface with huge mass enhancement as well as the transport anomalies in CeRhIn<sub>5</sub> under pressure are naturally explained from the viewpoint of the interplay of the AF order and Ce-valence fluctuations.

- 1) T. Moriya, *Spin Fluctuations in Itinerant Electron Magnetism* (Springer-Verlag, Berlin, 1985).
- 2) J. A. Hertz: Phys. Rev. B **14** (1976) 1165.
- 3) A. J. Millis: Phys. Rev. B **48** (1993) 7183.
- 4) W. Bao, P. G. Pagliuso, J. L. Sarrao, J. D. Thompson, Z. Fisk, J. W. Lynn, and R. W. Erwin: Phys. Rev. B **67** (2003) 099903.
- 5) H. Hegger, C. Petrovic, E. G. Moshopoulou, M. F. Hundley, J. L. Sarrao, Z. Fisk, and J. D. Thompson: Phys. Rev. Lett. **8** (2000) 4986.
- 6) T. Mito, S. Kawasaki, G.-q. Zheng, Y. Kawasaki, K. Ishida, Y. Kitaoka, D. Aoki, Y. Haga, and Y. Ōnuki: Phys. Rev. B **63** (2001) 220507.
- 7) T. Muramatsu, N. Tateiwa, T. C. Kobayashi, K. Shimizu, K. Amaya, D. Aoki, H. Shishido, Y. Haga, and Y. Ōnuki: J. Phys. Soc. Jpn. **70** (2001) 3362.
- 8) G. Knebel, M.-A. Méasson, B. Salce, D. Aoki, D. Braithwaite, J. P. Brison, and J. Flouquet: J. Phys.: Condens. Matter **16** (2004) 8905.
- 9) H. Shishido, R. Settai, H. Harima, and Y. Ōnuki: J. Phys. Soc. Jpn. **74** (2005) 1103.
- 10) T. Park, F. Ronning, H. Q. Yuan, M. B. Salamon, R. Movshovich, J. L. Sarrao, and J. D. Thompson: Nature **440** (2006) 65.
- 11) G. Knebel, D. Aoki, J. P. Brison, and J. Flouquet: J. Phys. Soc. Jpn. **77** (2008) 114704.
- 12) T. Park, V. A. Sidorov, F. Ronning, J.-X. Zhu, Y. Tokiwa, H. Lee, E. D. Bauer, R. Movshovich, J. L. Sarrao, and J. D. Thompson: Nature **456** (2008) 366.
- 13) H. Shishido, R. Settai, D. Aoki, S. Ikeda, H. Nakawaki, N. Nakamura, T. Iizuka, Y. Inada, K. Sugiyama, T. Takeuchi, K. Kindo, T. C. Kobayashi, Y. Haga, H. Harima, Y. Aoki, T. Namiki, H. Sato, and Y. Ōnuki: J. Phys. Soc. Jpn. **71** (2002) 162.
- 14) N. F. Phillips, R. A. Fisher, F. Bouquet, M. F. Hundley, P. G. Pagliuso, J. L. Sarrao, Z. Fisk, and J. D. Thompson: J. Phys.: Condens. Matter **15** (2003) S2095.
- 15) D. Jaccard, H. Wilhelm, K. Alami-Yadri, and E. Vargoz: Physica B **259-261** (1999) 1.
- 16) A. T. Holmes, D. Jaccard, and K. Miyake: Phys. Rev. B **69** (2004) 024508.
- 17) H. Q. Yuan, F. M. Grosche, M. Deppe, C. Geibel, G. Sparn, and F. Steglich: Science **302** (2003) 2104.

- 18) K. Fujiwara, Y. Hata, K. Kobayashi, K. Miyoshi, J. Takeuchi, Y. Shimaoka, H. Kotegawa, T. C. Kobayashi, C. Geibel, and F. Steglich: J. Phys. Soc. Jpn. **77** (2008) 123711.
- 19) W. E. Pickett, A. J. Freeman, and D. D. Koelling: Phys. Rev. B **23** (1981) 1266.
- 20) S. Watanabe, M. Imada, and K. Miyake: J. Phys. Soc. Jpn. **75** (2006) 043710.
- 21) S. Watanabe, A. Tsuruta, K. Miyake, and J. Flouquet: J. Phys. Soc. Jpn. **79** (2009) 104706.
- 22) Y. Onishi and K. Miyake: J. Phys. Soc. Jpn. **69** (2000) 3955.
- 23) K. Miyake: J. Phys.: Condens. Matter **19** (2007) 125201.
- 24) S. Watanabe, A. Tsuruta, K. Miyake, and J. Flouquet: Phys. Rev. Lett. **100** (2008) 236401.
- 25) K. Miyake and H. Maebashi: J. Phys. Soc. Jpn. **71** (2001) 1007.
- 26) G. Kotliar and A. E. Ruckenstein: Phys. Rev. Lett. **57** (1996) 1362.
- 27) D. Hall, E. C. Palm, T. P. Murphy, S. W. Tozer, C. Petrovic, E. M.-Ricci, L. Peabody, C. Q. H. Li, U. Alver, R. G. Goodrich, J. L. Sarrao, P. G. Pagliuso, J. M. Wills, and Z. Fisk: Phys. Rev. B **64** (2001) 064506.
- 28) K. Miyake, T. Matsuura, and C. M. Varma: Solid State Commun. **71** (1989) 1149.
- 29) R. Settai, H. Shishido, S. Ikeda, Y. Murakawa, M. Nakashima, D. Aoki, Y. Haga, H. Harima, and Y. Ōnuki: J. Phys.: Condens. Matter **13** (2001) L627.
- 30) L. D. Pham, T. Park, S. Maguion, J. D. Thompson, and Z. Fisk: Phys. Rev. Lett. **97** (2006) 056404.
- 31) S. Watanabe: J. Phys. Soc. Jpn. **69** (2000) 2947.
- 32) R. Daou, C. Bergemann, and S. R. Julian: Phys. Rev. Lett. **96** (2006) 026401.
- 33) K. Miyake and H. Ikeda: J. Phys. Soc. Jpn. **75** (2006) 033704.
- 34) M. Yashima, H. Mukuda, Y. Kitaoka, H. Shishido, R. Settai, and Y. Ōnuki: Phys. Rev. B **79** (2009) 214528.